

# One-transmitter Multiple-receiver Wireless Power Transfer System Using an Exceptional Point of Degeneracy

Fatemeh Mohseni<sup>1</sup>, Alireza Nikzamir<sup>1</sup>, Hung Cao<sup>1,2\*</sup>, Filippo Capolino<sup>1,3\*</sup>

<sup>1</sup>Electrical Engineering and Computer Science, University of California, Irvine, CA, USA

<sup>2</sup>Biomedical Engineering, University of California, Irvine, CA, USA

<sup>3</sup>Department of Communications and Signal Theory, University Carlos III of Madrid, Spain

**Abstract**— Robust transfer efficiency against the various operating conditions in a wireless power transfer system remains a fundamentally important challenge. This challenge becomes even more critical when transferring power to groups of inductively coupled receivers. We propose a method for efficient wireless power transfer to multiple receivers exploiting the concept of exceptional points of degeneracy (EPD). In previous studies based on PT symmetry, a receiver's operation has been divided into two strong and weak coupling regimes, and the power transfer efficiency is constant in the strong coupling regime when varying the coupling factor. Here the concept of strong and weak coupling and constant power efficiency is extended to a system of multiple receivers that do not follow PT symmetry. We show that the important feature to have a roughly constant power efficiency, independently of the positions of the receivers, is the existence of an EPD that separates the weak and strong regimes. Our proposed method demonstrates a system with less sensitivity to the coupling change than a conventional system without EPD when the receivers and their couplings to the transmitter are not necessarily identical.

**Keywords**—Wireless Power Transfer; Exceptional Points of Degeneracy; Inductive Coupling.

## I. INTRODUCTION

Wireless power transfer (WPT) has paved the way for recent advances in portable electronic devices in a host of applications, from eliminating the dominance of the battery on biomedical devices to wirelessly powered laptops needless of charging wires [1]. Methods can be categorized into two main classes: radiative and non-radiative WPT. Like far-field or RF broadcast techniques, radiative WPT is based on propagating electromagnetic waves carrying energy. Although they are suitable for transferring data, there are certain disadvantages for transmitting power, *e.g.*, in far-field approaches, the efficiency

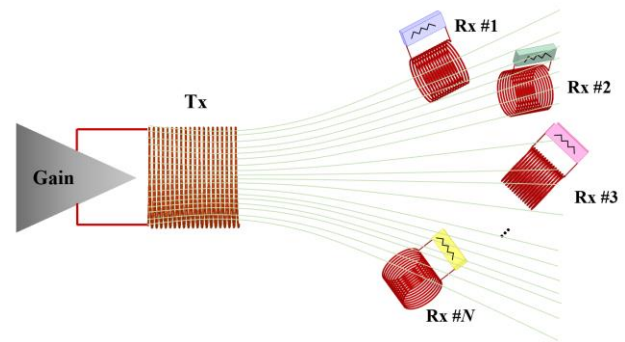


Fig. 1. Wireless power transfer from one transmitter (Tx) to  $N$  receivers (Rx) inductively coupled. The system exhibits an exceptional point of degeneracy.

depends on the transmitter's directivity. Although in RF broadcasting methods, this is solved by omnidirectional propagation, the transferred power drops rapidly by increasing distance due to the  $1/r^2$  dependency. Therefore, non-radiative methods like inductive coupling based on resonant LC tanks are becoming more widespread [2]. Nowadays, inductive WPT can be found in a variety of devices, such as biomedical implants [3], electric automobiles [4], household appliances [5], and laboratory research[6].

Previous studies proved the potential of WPT using a magnetic inductive link [7][8][9]. Two magnetically coupled resonators, one on the source side and one on the reception side, make up a primary near-field wireless power transmission system. The rates at which energy is injected into and taken out of each resonator and the frequency of the source resonator are all carefully adjusted to ensure efficient power transfer. However, since the change in distance and the relative

positioning of the transmitter and receiver affect the coupling factor, the efficiency is out of control in practical scenarios. Therefore, reaching robust WPT without the need for active tuning to get the optimal efficiency is a challenge in designing systems that require dynamic charging. One of the effective methods to solve this problem is using parity-time (PT) symmetric circuits with a nonlinear gain in one resonator, which could balance the loss on the other one [10], [11]. Assaworarith *et al.* [12] have demonstrated that in WPT links with one receiver possessing PT-symmetry conditions with nonlinear saturation, the system could self-select the operation frequency with optimal efficiency. The PT-symmetry condition can be achieved through a composite gain/loss system which is invariant under the parity (P) and time-reversal (T) operators. The PT-symmetric system made of two resonators has two phases: i) the 'unbroken phase' in which the frequency spectrum is real, and the energy is stored equally between gain and loss regions; and ii) the 'broken phase' in which the eigenfrequencies are complex; therefore, while one mode is growing exponentially, the other one decreases [13]–[18]. In some systems, these two regions are defined based on exceptional points of degeneracy (EPD) [19]. An EPD is a special point in a system parameter space at which two or more eigenmodes coalesce in both their eigenvalues and eigenvectors into a single degenerate eigenmode by varying frequency or other parameters of the system [20]–[24]. The main feature of an exceptional point is the strong full degeneracy of the relevant eigenmodes, justifying the presence of "D" in EPD, which stands for "degeneracy" [25]. In order to have the EPD, the power generation rate in the transmitter and the power dissipation rate in the receivers should reach a balance.

In this paper, first, we summarize the concept of exceptional points of degeneracy (EPD) in multiple resonator systems using coupled-mode theory. **Fig. 1** shows the general concept of using inductive coupling to transfer power to multiple receivers. We use the EPD characteristics to reach an approximately constant efficiency region in a non-PT-symmetric system for power transfer to more than one receiver, assuming that the resonators and their couplings to the main transmitter are not necessarily identical. This method shows that no PT-symmetry condition is required; the WPT system needs to have an EPD, separating the strong and weak coupling regions. Finally, we theoretically and experimentally demonstrate the method for a WPT system made of one transmitter and two receivers, but the theory presented here is also valid for  $N$ -receiver systems.

## II. EPD CONDITION FOR WIRELESS POWER TRANSFER TO MULTIPLE RECEIVERS

The system in **Fig. 1** with  $N$  receivers is described using coupled-mode theory [4] as

$$\dot{a}_m(t) = (i\omega_m - \gamma_m + g_{\text{gain}}\delta_{m0})a_m(t) + \sum_{n \neq m} iK_{mn}a_n(t) + s_m(t). \quad (1)$$

$a_m$  is the complex mode amplitude in the  $m$ -th resonator, defined such that  $|a_m|^2$  represents the energy stored in such

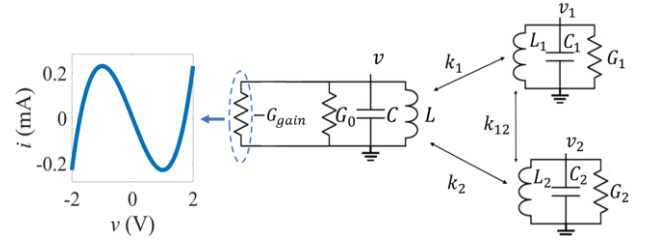


**Fig. 2.** WPT scheme with three coupled resonators. Power in the transmitter is provided by nonlinear gain  $-G_{\text{gain}}$ , with the shown  $i - v$  curve. The two receiver resonators are terminated with linear conductance  $G_1$  and  $G_2$ , respectively.

resonator, with  $m = 0, 1, 2, \dots, N$ . In Eq. (1),  $\delta_{m0}$  is the Kronecker delta, which is equal to 1 if  $m = 0$  and zero otherwise. We assume every quantity has a time evolution  $a_m \propto e^{i\omega t}$  where  $\omega$  is the considered angular frequency. The term  $s_m$  is the possible source in each resonator which, though in our case, we assume that there are no sources since we look at the eigenfrequencies of the system and the self-oscillatory regime induced by the presence of gain. The angular eigenfrequency of the uncoupled (i.e., isolated)  $m$ -th resonator is  $\omega_m = 1/\sqrt{L_m C_m}$ , and  $\gamma_m = G_m \omega_m \sqrt{L_m / C_m}$  is the loss factor. The factor  $K_{mn} = \omega_m k_{mn}$ , with  $k_{mn} = M_{mn} / \sqrt{L_m L_n}$ , is the coupling coefficient between the  $m$ -th and the  $n$ -th resonators, and  $M_{mn}$  is their mutual inductance. The transmitter is denoted by  $m = 0$ , whereas the  $N$  receivers are denoted by  $m = 1, 2, 3, \dots, N$ .

To simplify the notation and the experimental demonstration, in the rest of the paper, we will focus on the WPT case with one transmitter and two receivers, with inductive magnetic couplings as in **Fig. 2**. The coupling factor between the transmitter and two receivers is  $k_{01}$  and  $k_{02}$ ; for the sake of brevity, we will instead use  $k_1$  and  $k_2$ , respectively. We consider the effective gain  $-g = -g_{\text{gain}} + \gamma_0$  in the transmitter, where  $g_{\text{gain}} = G_{\text{gain}} \omega_0 \sqrt{L/C}$ , and  $\omega_0 = 1/\sqrt{LC}$  is the uncoupled (i.e., isolated) transmitter resonant angular frequency and  $\gamma_0$  is the intrinsic loss rate in the transmitter. The negative conductance  $-G_{\text{gain}}$  is easily realized using electronic components. Based on the coupled-mode theory for the schematic in **Fig. 2**, the system equations assuming matched resonance before coupling (i.e.,  $\omega_1 = \omega_2 = \omega_0$ ) are

$$\frac{d}{dt} \begin{bmatrix} a \\ a_1 \\ a_2 \end{bmatrix} = \begin{bmatrix} i\omega_0 + g & iK_1 & iK_2 \\ iK_1 & i\omega_0 - \gamma_1 & iK_{12} \\ iK_2 & iK_{12} & i\omega_0 - \gamma_2 \end{bmatrix} \begin{bmatrix} a \\ a_1 \\ a_2 \end{bmatrix}. \quad (2)$$

For ease of the demonstration, we choose the receivers' loss rates as  $\gamma_1 = \gamma_2 = \gamma_r$ . We further neglect the effect of mutual coupling between the two receivers ( $k_{12} = 0$ ) since they have very small inductors and are not necessarily close to each other in practical scenarios. The system has three eigenfrequencies

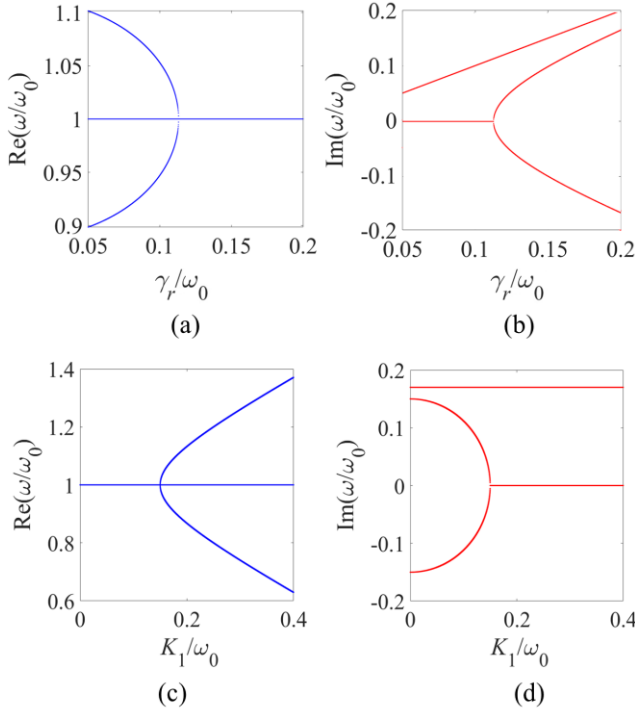


**Fig. 3.** (a) Real and (b) imaginary parts of the angular eigenfrequencies of the system in Fig. 2 versus the loss rate in the receivers  $\gamma_r$ , assuming  $g = \gamma_r$ . The EPD of order two (the bifurcation point) happens at  $\gamma_r/\omega_0 = 0.17$ , while  $K_1/\omega_0 = K_2/\omega_0 = 0.124$ , where the eigenvalues of the system coalesce. (c) Real and (d) imaginary parts of angular eigenfrequencies versus coupling rate to receiver #1 with constant  $K_2/\omega_0 = 0.08$  and  $\gamma_r/\omega_0 = 0.17$ . The EPD occurs at  $K_{1,e}/\omega_0 = 0.15$ .

that are found by solving the eigenvalue problem associated with the matrix of Eq. (2), leading to

$$\omega_i = \left\{ \begin{array}{l} \omega_0 - \frac{i\gamma_r}{2} + \frac{ig}{2} - \frac{1}{2} \sqrt{-g^2 - 2g\gamma_r + 4K_1^2 + 4K_2^2 - \gamma_r^2} \\ \omega_0 - \frac{i\gamma_r}{2} + \frac{ig}{2} + \frac{1}{2} \sqrt{-g^2 - 2g\gamma_r + 4K_1^2 + 4K_2^2 - \gamma_r^2} \end{array} \right\}. \quad (3)$$

If we choose the gain conductance as  $g = \gamma_r$  to have the balance between the gain and loss, two of the three eigenfrequencies will be real and equal to each other when

$$\gamma_r = \sqrt{K_2^2 + K_1^2}. \quad (4)$$

Equation (4) is the condition for the system to exhibit an EPD of order two that occurs at  $\omega_e = \omega_0$ . The coalescence of the eigenvalues and eigenvectors is a necessary condition for an EPD to exist. Without resorting to the demonstration that two eigenvectors coalesce, we instead show that the two perturbed eigenvalues exhibit the typical square root-like (second-order EPD) behavior when they bifurcate at the EPD. Indeed, when varying the loss factor in the receivers, **Fig. 3** shows a second-order EPD in the system. This EPD represents a separation between the strong and weak coupling regimes. Therefore, if

the values of  $R$ ,  $L$ , and  $C$  values in each receiver meet the condition of equal loss rate  $\gamma_1 = \gamma_2 = \gamma_r$ , even though each resonator has different inductance and capacitance, the EPD still exists. For coupling values of  $K_1$  and  $K_2$  such that  $\sqrt{K_2^2 + K_1^2} > \gamma_r$ , the system is in a strong coupling regime. Under this regime, the system supports two modes with *real* frequencies  $\omega_0 \pm \sqrt{K_1^2 + K_2^2 - \gamma_r^2}$ , and one complex eigenfrequency  $\omega_0 + i\gamma_r$ . Due to the imaginary part, the  $\omega_0 + i\gamma_r$  mode is decaying over time. Due to the nonlinear gain in the transmitter, the mode that requires the least gain will grow to attain its steady state and saturate out the gain, preventing other modes from gaining access to the gain required for steady-state oscillation.

### III. THEORETICAL WIRELESS POWER TRANSFER EFFICIENCY

To analyze the total power transferred to both receivers' loads, the total power efficiency  $\eta_t$  is calculated for different ranges of coupling using coupled-mode theory [26] as

$$\eta_t = \frac{\gamma_1 |a_1|^2 + \gamma_2 |a_2|^2}{\gamma_0 |a|^2 + \gamma_1 |a_1|^2 + \gamma_2 |a_2|^2} = \left\{ \begin{array}{ll} \frac{\gamma_r}{\gamma_r + \gamma_0} & , \quad \gamma_r \leq \sqrt{K_2^2 + K_1^2} \\ \frac{K_1^2 + K_2^2}{K_1^2 + K_2^2 + \gamma_r \gamma_0} & , \quad \gamma_r > \sqrt{K_2^2 + K_1^2} \end{array} \right\}. \quad (5)$$

In the strong coupling regime, the total efficiency is independent of the coupling factors, and when the intrinsic loss rates are negligible, it approaches unity. Since we have two possibly varying coupling factors, there is a two dimensional (2-D) strong coupling region as shown in **Fig. 4** (outside the white-dashed circle of radius  $\gamma_r/\omega_0$ , leading to high efficiency. In the weak coupling regime, the coupling factor variation

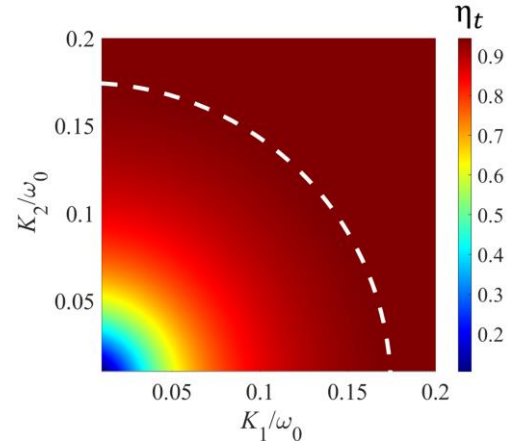


**Fig. 4.** Total efficiency and strong (inner) and weak (outer) coupling regions separated by the dashed-white circle. The dashed-white circle represents the EPD condition  $K_2^2 + K_1^2 = \gamma_r^2$  which defines the boundary between the two coupling regimes with the values of  $\gamma_r/\omega_0 = 0.17$  and  $\gamma_0/\omega_0 = 0.001$ .

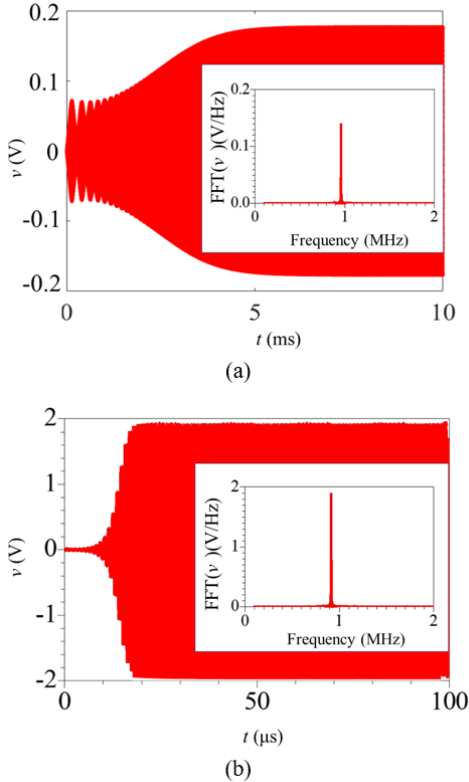


**Fig. 5.** Time-domain signal  $v(t)$  in transmitter after reaching saturation due to the nonlinear effects of the active element showing a single frequency of oscillation, and frequency spectrum. (a) System operating at the EPD, with oscillation frequency very close to  $f_e = 0.959$  MHz. (b) System operating away from the EPD, in the strong coupling regime, when  $k_1 = 0.2$  and  $k_2 = 0.08$ . In this case, there is still one single oscillating frequency at  $f = 0.912$  MHz.

changes the total power efficiency of both receivers. The details of the efficiency calculation are explained in Appendix A.

To analyze the power transferred to each resonator individually, the other resonator is assumed to be fixed. For example, assuming  $K_2$  constant and such that  $K_2 < \gamma_r$ , we define  $K_{1,e} = \sqrt{\gamma_r^2 - K_2^2}$  as the EPD condition for different coupling regions in receiver #1 based on Eq. (4); the strong coupling regime  $K_1 > K_{1,e}$  is now explicitly defined for receiver #1, but the same calculation process is also valid for the second receiver. Still assuming  $K_2$  constant, the efficiency for receiver #1 is written as

$$\eta_1 = \frac{\gamma_1 |a_1|^2}{\gamma_0 |a|^2 + \gamma_1 |a_1|^2 + \gamma_2 |a_2|^2} = \left\{ \begin{array}{ll} \frac{\gamma_r}{\gamma_r + \gamma_0} \frac{K_1^2}{K_1^2 + K_2^2}, & K_1 \geq K_{1,e} \\ \frac{K_1^2}{K_1^2 + K_2^2 + \gamma_r \gamma_0}, & K_1 < K_{1,e} \end{array} \right\}. \quad (6)$$

Assuming  $K_2 < \gamma_r$ , in the strong coupling regime  $K_1 > K_{1,e}$  the power delivered to receiver #1 does not vary drastically

with the change in  $K_1$  and remains roughly constant despite changes in its coupling factor with the transmitter for a range such that  $K_1 \gg K_2$ . In the weak coupling for the first receiver, when  $K_1 < K_{1,e}$ , the effect of coupling change on receiver #1 efficiency is more significant.

In the case that  $K_2 > \gamma_r$ , the operating points for both receivers are outside the white dashed circle in Fig. 4. Since both receivers are in the strong coupling regime, both  $K_1$  and  $K_2$  have a considerable impact on the *individual* efficiency. Indeed, when varying  $K_1$  the system does not experience any EPD point, and the efficiency for receiver #1 does not level to a constant value. The same analysis is valid for receiver #2 when fixed  $K_1$  is chosen such that  $K_1 > \gamma_r$ .

Also, considering the operating point position in Fig. 4, summation of the two individual efficiencies,  $\eta_t = \eta_1 + \eta_2$  yields Eq. (5).

#### IV. POWER TRANSFER EFFICIENCY

The negative conductance feeds power to the transmitter resonator, which is coupled through a magnetic link to the receivers with loads denoted by  $G_1$  and  $G_2$  in Fig. 2. The transient behavior of the system is obtained by using the time-domain (TD) circuit simulator Keysight ADS with the initial condition at the transmitter  $v(t=0) = 1$  mV. The parameters in the Tx part are  $C = 330$  pF,  $L = 84.45$   $\mu$ H,  $G_{gain} = 0.345$  mS,  $G_0 = 0.002$  mS, and the Rx parameters are  $C_1 = C_2 = 3.30$  nF,  $L_1 = L_2 = 8.445$   $\mu$ H,  $G_1 = G_2 = 3.45$  mS. The other intrinsic losses in the resonators in receivers are negligible. These circuit parameters lead to the values of  $\gamma_r/\omega_0 = 0.17$  and  $\gamma_0/\omega_0 = 0.001$ ; hence satisfy the EPD condition discussed in the previous section.

The gain element is realized using a cubic model with an  $i - v$  curve described as  $i = -G_{gain}v + \alpha v^3$ ; where  $-G_{gain}$  is the negative slope of  $i - v$  curve in the negative admittance region, and  $\alpha$  is the third-order non-linearity constant that models the saturation characteristic of the device [27]. The value of the saturation characteristic  $\alpha$  determines the steady-state saturation amplitude, and we set it as  $\alpha = G_{gain}/3$ .

Fig. 5(a) shows the TD circuit simulation of the capacitor voltage  $v(t)$  in the transmitter when  $k_1 = k_2 = 0.124$ , i.e., when the system is supposed to operate at the EPD. The frequency spectrum of the transmitter voltage, after reaching saturation, shows a fundamental operating frequency of oscillation  $f_{osc} = 0.963$  MHz, very close to  $f_e = 0.959$  MHz (linear regime). The small difference comes from using nonlinear gain used in the TD simulation. The frequency spectrum of the TD voltage signal  $v(t)$  at the transmitter's capacitor, after reaching saturation, is obtained by applying the fast Fourier transform (FFT) of the TD signal. The FFT is calculated using  $10^6$  samples in the time window from 5 ms to 10 ms. Fig. 5(b) demonstrates the transmitter's TD signal in simulation, away from EPD, with  $k_1 = 0.2$  and  $k_2 = 0.08$ , i.e., in the strong coupling regime. After reaching saturation, the self-oscillating frequency for this case is  $f = 0.912$  MHz, based on the FFT of the TD signal. Note that there are two real

eigenfrequencies in the strongly coupled regime in the linear regime. However, the spectrum of the signal of the nonlinear simulation shows only one frequency of oscillation. This is because the nonlinear gain slightly perturbs the system away from the ideal condition, and one resonance dominates (i.e., it becomes unstable) over the other in the saturation process.

The experimental verification discussed next is based on the setup shown in **Fig. 6(a)**. It uses the same conductances and LC parameters as the circuit simulation values for the transmitter and receivers.

As a preliminary step, after the three inductors had been fabricated, we fine-tuned the transmitter's capacitance so that the transmitter's resonance frequency matches that of the two uncoupled resonators, using a rack of capacitors. A resistance trimmer was used to adjust the value of the gain rate to the value of  $-G_{gain}$  in the transmitter, based on the calculated value of the required gain derived from theory for the system to have an EPD. The detail for tuning is explained in Appendix C. Then, we used an oscilloscope to measure the TD response of the voltage signal in the resonators. We also used a spectrum analyzer to examine the frequency response, and confirmed that the three coupled-coil system, including the active nonlinear component, works in the proximity of the EPD. **Fig. 6(b)** shows the operating self-oscillation frequency in the configuration with receiver #1 moving while receiver #2 is fixed. As it is demonstrated, the operating frequency starts varying when the coupling to receiver #1 gets close to the EPD value ( $k_1$  getting close to  $k_{1,e}$ ) and it keeps changing in the strong coupling region ( $k_1 > k_{1,e}$ ). The FFT spectrum from the simulated TD signal is well matched to the experimental spectrum (either obtained from the oscilloscope waveform and the spectrum analyzer) for all values of coupling  $k_1$  in the range of 0-0.3. There is a transition of the steady-state frequency among the frequency branches around the EPD in the measurement. This transition has little effect on transfer efficiency. It can result from: i) minor resonator mistune, ii) the detuning due to the nonlinear part when we have the saturation and iii) the difference between the initial value for gain in measurement and theory.

To investigate the features of power efficiency of the WPT system with EPD, we move one of the receivers' coils (e.g., receiver #1) to determine the transmitter and receivers' power changes while keeping the other receiver (e.g., receiver #2) fixed. The distance range between the transmitter and receivers' coils in the test is converted to the coupling coefficients by using the relation between the coupling coefficient and the distance between coils, as shown in **Fig. 9** in appendix C. Efficiency is defined as the power received by the two receivers to the power generated in the transmitter by the nonlinear active element. The power received by the two receivers is obtained by measuring the voltage on each receiver and calculating power as  $(V_i^2 G/2)$  for  $i = 1,2$ . The experiment was repeated with different distances between receiver #2 (the stationary one) and the transmitter to investigate the effect of the fixed receiver position on the moving receiver's efficiency. The measurement distance for the coupling range is in the interval of 5-30 mm.

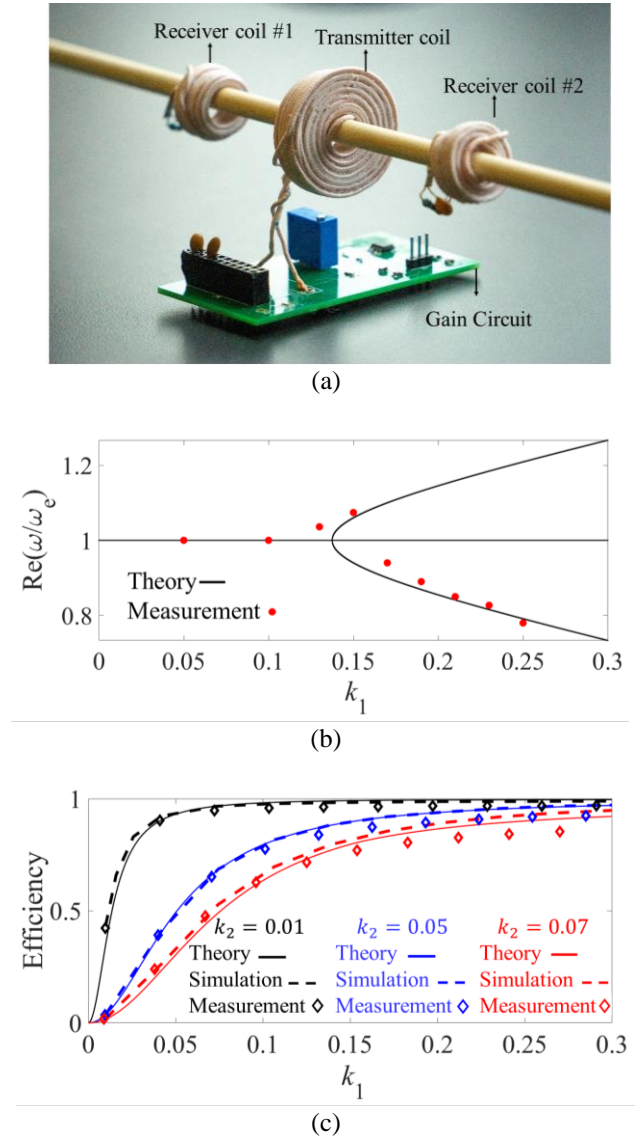


**Fig. 6** (a). Setup used in measurement of the power transfer efficiency for receiver #1, defined in Eq. (6). (b) Real part of normalized angular eigenfrequencies versus the coupling rate to the receiver #1, with constant  $k_2 = 0.08$ . The theoretical value (using linear gain) shows two real frequencies in the strong coupling regime. The measurement shows the steady state self-oscillation frequency, when using nonlinear gain. Only one frequency is observed for every coupling coefficient. (c) Power efficiency for receiver #1 varying the coupling factor  $k_1$ , with three constants  $k_2$  values:  $k_2 = 0.01$  (black),  $k_2 = 0.05$  (blue),  $k_2 = 0.07$  (red). Solid lines represent the theory calculation with linear gain, dashed lines are obtained from timed domain simulations with nonlinear gain, and the diamond symbols are for measurements.

Results in **Fig. 6(c)** are calculated as follows: the theory is based on Eq. (6); simulations and circuit measurements are based on the steady-state saturated regime caused by the nonlinear active gain. The simulated and measurement results agree with the theory from the coupled-mode theory calculation. The results show that the receiver's efficiency after

the EPD (i.e., in the strong coupling regime) is almost constant, and approximately independent of the value of the coupling coefficient  $k_1$ . **Figure 6(c)** also shows that the value of the second receiver's coupling factor  $k_2$  affects the maximum efficiency value for receiver #1. As the second receiver gets closer to the transmitter,  $k_2$  increases, and the efficiency of the first receiver decrease since the second receiver draws more power from the transmitter. However, the transferred energy to receiver #1 is still approximately constant over the strong coupling range  $K_1 > K_{1,e}$ . Also, the location of receiver #2 (i.e., the value of the coupling factor  $k_2$ ) changes the EPD in the system and consequently redefines the strong-weak coupling region for receiver #1.

In the theoretical calculations and TD circuit simulations, the passive circuit elements in the receiver have been considered lossless. The slight difference between the value of efficiency in simulation and measurement could be addressed by the presence of losses in the system, such as the intrinsic loss of the coils and the extra loss from the circuit elements and measurement pin joints.

## V. CONCLUSION

We have proposed a new efficient wireless power transfer method involving one transmitter and multiple receivers exploiting the EPD concept in a non-PT-symmetric structure. This method provides a coupling-independent eigenfrequency region, leading to the design of a system that can transfer power to multiple moving receivers without requiring active tuning of circuit parameters. Analyses of relatively simple implementation geometries show promising performance characteristics, and substantial design tuning is predicted to yield even better results.

A finely tuned EPD point enables a range of constant efficiency without the need for extra electronic circuits in receivers. Moreover, since the receivers and transmitter do not necessarily need to be identical in our proposed method, our method can be useful in a wide range of practical applications, including passive wireless sensing from multiple sites [6], and powering multiple compact implants and microrobots [3].

## APPENDIX A: POWER TRANSFER EFFICIENCY

In this section, we calculate the expressions for power transfer efficiency based on the coupled-mode theory equations. Using Eq. (1), for a system made of one transmitter and two receivers, and assuming all quantities include the complex time-varying factor  $\exp(i\omega t)$ , we have:

$$i\omega a = (i\omega_0 + g)a + iK_1a_1 + iK_2a_2, \quad (7)$$

$$i\omega a_1 = (i\omega_1 - \gamma_1)a_1 + iK_1a + iK_{12}a_2, \quad (8)$$

$$i\omega a_2 = (i\omega_2 - \gamma_2)a_2 + iK_2a + iK_{12}a_1. \quad (9)$$

Assuming  $K_{12} = 0$ , the  $a_1$  and  $a_2$  mode amplitudes in each receiver resonator are calculated as

$$a_1 = \frac{iK_1}{i(\omega - \omega_1) - \gamma_1} a, \quad (10)$$

$$a_2 = \frac{iK_2}{i(\omega - \omega_2) - \gamma_2} a. \quad (11)$$

In the following, we assume that all three resonator's natural frequencies (when uncoupled) are matched, i.e.,  $\omega_1 = \omega_2 = \omega_0$ .

When the operating frequency  $\omega$  is such that  $\omega = \omega_0$  (which is valid in the weak coupling regime, and only as an approximation in the strong coupling regime), we can evaluate  $a_1$  and  $a_2$  in very simple terms as

$$a_1 = \frac{iK_1}{-\gamma_1} a, \quad (12)$$

$$a_2 = \frac{iK_2}{-\gamma_2} a. \quad (13)$$

Above, we did not consider the complex frequency solution in Eq. (3) because it decays exponentially. The efficiency is calculated based on the power delivered to the receivers to the total power generated, which is equal to the power dissipated by the receivers' loads and the intrinsic loss in the transmitter. The total efficiency, assuming  $\gamma_1 = \gamma_2 = \gamma_r$ , in the weak coupling regime is

$$\begin{aligned} \eta_t &= \frac{\text{Power transferred to both receivers}}{\text{Total power generated}} \\ &= \frac{\gamma_1|a_1|^2 + \gamma_2|a_2|^2}{\gamma_0|a|^2 + \gamma_1|a_1|^2 + \gamma_2|a_2|^2} \\ &= \frac{\gamma_1 \left| \frac{K_1}{\gamma_1} \right|^2 |a|^2 + \gamma_2 \left| \frac{K_2}{\gamma_2} \right|^2 |a|^2}{\gamma_0|a|^2 + \gamma_1 \left| \frac{K_1}{\gamma_1} \right|^2 |a|^2 + \gamma_2 \left| \frac{K_2}{\gamma_2} \right|^2 |a|^2} \\ &= \frac{K_1^2 + K_2^2}{K_1^2 + K_2^2 + \gamma_r \gamma_0}. \end{aligned} \quad (14)$$

The efficiency of each individual receiver can be derived following an analogous procedure. For example, the efficiency for receiver #1 in the weak coupling regime is

$$\begin{aligned} \eta_1 &= \frac{\text{Power transferred to receiver #1}}{\text{Total power generated}} \\ &= \frac{\gamma_1|a_1|^2}{\gamma_0|a|^2 + \gamma_1|a_1|^2 + \gamma_2|a_2|^2} \\ &= \frac{\gamma_1 \left| \frac{K_1}{\gamma_1} \right|^2 |a|^2}{\gamma_0|a|^2 + \gamma_1 \left| \frac{K_1}{\gamma_1} \right|^2 |a|^2 + \gamma_2 \left| \frac{K_2}{\gamma_2} \right|^2 |a|^2} \\ &= \frac{K_1^2}{K_1^2 + K_2^2 + \gamma_r \gamma_0}. \end{aligned} \quad (15)$$

In the strong coupling regime, we use the precise value of the eigenfrequencies  $\omega = \omega_0 \pm \sqrt{K_1^2 + K_2^2 - \gamma_r^2}$  and we still assume  $\omega_1 = \omega_2 = \omega_0$  and  $\gamma_1 = \gamma_2 = \gamma_r$ . Therefore, using Eqs. (10) and (11),  $a_1$  and  $a_2$  in strong coupling are

$$a_1 = \frac{iK_1}{\mp i\sqrt{K_1^2 + K_2^2 - \gamma_r^2} - \gamma_r} a, \quad (16)$$

$$a_2 = \frac{iK_2}{\mp i\sqrt{K_1^2 + K_2^2} - \gamma_r^2 - \gamma_r} a. \quad (17)$$

And the magnitude of  $a_1$  and  $a_2$  is

$$|a_1| = \frac{K_1}{\sqrt{K_1^2 + K_2^2}} |a|, \quad (18)$$

$$|a_2| = \frac{K_2}{\sqrt{K_1^2 + K_2^2}} |a|. \quad (19)$$

Substituting Eqs. (18) and (19) in the efficiency formula, the total efficiency in the strong coupling is

$$\begin{aligned} \eta_t &= \frac{\gamma_1 |a_1|^2 + \gamma_2 |a_2|^2}{\gamma_0 |a|^2 + \gamma_1 |a_1|^2 + \gamma_2 |a_2|^2} \\ &= \frac{\gamma_1 \left| \frac{K_1}{\sqrt{K_1^2 + K_2^2}} \right|^2 |a|^2 + \gamma_2 \left| \frac{K_2}{\sqrt{K_1^2 + K_2^2}} \right|^2 |a|^2}{\gamma_0 |a|^2 + \gamma_1 \left| \frac{K_1}{\sqrt{K_1^2 + K_2^2}} \right|^2 |a|^2 + \gamma_2 \left| \frac{K_2}{\sqrt{K_1^2 + K_2^2}} \right|^2 |a|^2} \\ &= \frac{\gamma_r}{\gamma_r + \gamma_0}. \end{aligned} \quad (20)$$

Therefore, the total efficiency in the strong coupling region is not dependent on the couplings with the transmitter.

Analogously, for the individual receiver #1 in the strong coupling  $K_1 > K_{1,e}$ , the efficiency is

$$\begin{aligned} \eta_1 &= \frac{\gamma_1 |a_1|^2}{\gamma_0 |a|^2 + \gamma_1 |a_1|^2 + \gamma_2 |a_2|^2} \\ &= \frac{\gamma_1 \left| \frac{K_1}{\sqrt{K_1^2 + K_2^2}} \right|^2 |a|^2}{\gamma_0 |a|^2 + \gamma_1 \left| \frac{K_1}{\sqrt{K_1^2 + K_2^2}} \right|^2 |a|^2 + \gamma_2 \left| \frac{K_2}{\sqrt{K_1^2 + K_2^2}} \right|^2 |a|^2} \\ &= \frac{\gamma_r}{\gamma_r + \gamma_0} \frac{K_1^2}{K_1^2 + K_2^2}. \end{aligned} \quad (21)$$

In the strong coupling regime, receiver #1's efficiency depends on both coupling factors with the transmitter. However, depending on the value of  $K_2$ , the efficiency can be approximately constant for  $K_2 < \gamma_r$ . Since in the strong coupling regime, the value for  $K_1$  is larger than  $K_2$ , there is no significant variation in efficiency. A similar analysis holds for receiver #2 as well.

## APPENDIX B: NONLINEAR GAIN AND STABILITY ANALYSIS

When the gain element is nonlinear, the gain saturates as the relative complex mode amplitude  $|a|$  increases, and the coupled-mode equations can have multiple steady-state solutions [28]. However, with the nonlinear gain model, the mode requiring the lowest gain will grow to reach its steady-state and saturate out the gain, preventing other modes from accessing the gain level they need to reach steady-state

oscillation. In this section, we provide an analysis of stability using the Lyapunov exponent behavior and demonstrate that the system settles into a steady state within a few cycles. The EPD is designed to be at a steady state.

We do not seek the general solutions of the differential equation of Eq. (1) for transient behaviour in the presence of nonlinear gain; indeed, to avoid such difficulty, we assume we work in a neighborhood of a saturated regime; hence we know the saturated mode amplitudes in the transmitter  $\tilde{a}$  and receivers  $\tilde{a}_1$  and  $\tilde{a}_2$ . We consider the perturbation for the transmitter as  $\rho \propto e^{\lambda t}$  and for receivers as  $\rho_{1,2} \propto e^{\lambda t}$  (where  $\lambda$  is the Lyapunov exponent) applied around the steady-state response, and we want to check if it vanishes over time; hence we check if the system is stable in a small neighborhood of the saturated regime. Therefore, for the two receivers' system in **Fig. 2**, we have

$$a = \tilde{a} + \rho, \quad (22)$$

$$a_1 = \tilde{a}_1 + \rho_1, \quad (23)$$

$$a_2 = \tilde{a}_2 + \rho_2. \quad (24)$$

We assume that the nonlinear dependency of the gain is  $g(|a/\tilde{a}|) = -\gamma_0 + 2(\gamma_r + \gamma_0)/(1 + |a/\tilde{a}|^2)$ . With this model, when the value of the mode amplitude  $a$  gets to the saturation value  $\tilde{a}$ , the saturated gain will be  $g = \gamma_r$  which is a condition for the system to have the EPD.

To solve Eq. (1) under this condition, we need to linearize the gain around the steady-state response using the Taylor expansion and omitting quadratic and higher order terms of  $\rho$ :

$$\begin{aligned} g(|a/\tilde{a}|) &= -\gamma_0 + 2 \frac{\gamma_r + \gamma_0}{1 + |a/\tilde{a}|^2} \\ &= -\gamma_0 + \frac{2(\gamma_r + \gamma_0)}{1 + (\tilde{a} + \rho)(\tilde{a} + \rho)^*/|\tilde{a}|^2} \\ &\approx -\gamma_0 + (\gamma_r + \gamma_0) \left( 1 - \frac{\tilde{a}\rho^* + \tilde{a}^*\rho}{|\tilde{a}|^2} \right). \end{aligned} \quad (25)$$

Now, with this linear estimation of the gain, the coupled-mode theory for the first resonator is written as

$$\begin{aligned} \frac{d}{dt}(\tilde{a} + \rho) &= [i(\omega_0 - \omega) + g(|a/\tilde{a}|)](\tilde{a} + \rho) \\ &\quad - iK_1(\tilde{a}_1 + \rho_1) - iK_2(\tilde{a}_2 + \rho_2). \end{aligned} \quad (26)$$

which leads to

$$\begin{aligned} \frac{d}{dt}\tilde{a} + \frac{d}{dt}\rho &= i(\omega_0 - \omega)\tilde{a} + i(\omega_0 - \omega)\rho \\ &\quad + g(|a/\tilde{a}|)\tilde{a} + g(|a/\tilde{a}|)\rho \\ &\quad - iK_1\tilde{a}_1 - iK_1\rho_1 - iK_2\tilde{a}_2 - iK_2\rho_2. \end{aligned} \quad (27)$$

$$\begin{aligned} \frac{d}{dt} \tilde{a} + \frac{d}{dt} \rho &= i(\omega_0 - \omega) \tilde{a} + i(\omega_0 - \omega) \rho \\ &+ \left[ (\gamma_r + \gamma_0) \left( 1 - \frac{\tilde{a} \rho^* + \tilde{a}^* \rho}{|\tilde{a}|^2} \right) - \gamma_0 \right] (\tilde{a}) \\ &+ \left[ (\gamma_r + \gamma_0) \left( 1 - \frac{\tilde{a} \rho^* + \tilde{a}^* \rho}{|\tilde{a}|^2} \right) - \gamma_0 \right] (\rho) \\ &- iK_1 \tilde{a}_1 - iK_1 \rho_1 - iK_2 \tilde{a}_2 - iK_2 \rho_2. \end{aligned} \quad (28)$$

Recalling that  $a_1 = \tilde{a}_1 + \rho_1$  and  $a_2 = \tilde{a}_2 + \rho_2$  and omitting the quadratic terms of  $\rho$ , we obtain the three linearized differential equations for perturbation

$$\frac{d}{dt} \rho = B_1 \rho + B_2 \rho^* + C_1 \rho_1 + C_2 \rho_2, \quad (29)$$

$$\frac{d}{dt} \rho_1 = D_1 \rho_1 + C_1 \rho, \quad (30)$$

$$\frac{d}{dt} \rho_2 = D_2 \rho_2 + C_2 \rho, \quad (31)$$

where

$$B_1 = i(\omega_0 - \omega) + \gamma_r - (\gamma_r + \gamma_0), \quad (32)$$

$$B_2 = -(\gamma_r + \gamma_0) \frac{\tilde{a}^2}{|\tilde{a}|^2}, \quad (33)$$

$$C_1 = -iK_1, \quad (34)$$

$$C_2 = -iK_2, \quad (35)$$

$$D_1 = i(\omega_1 - \omega) - \gamma_r, \quad (36)$$

$$D_2 = i(\omega_2 - \omega) - \gamma_r. \quad (37)$$

Assuming that the perturbations have the time dependency as [28]

$$\rho = u e^{\lambda t} + v^* e^{\lambda^* t}, \quad (38)$$

$$\rho_1 = u_1 e^{\lambda t} + v_1^* e^{\lambda^* t}, \quad (39)$$

$$\rho_2 = u_2 e^{\lambda t} + v_2^* e^{\lambda^* t}. \quad (40)$$

The linear system in matrix form from the above differential equations is

$$\begin{bmatrix} B_1 & B_2 & C_1 & 0 & C_2 & 0 \\ B_2^* & B_1^* & 0 & C_1^* & 0 & C_2^* \\ C_1 & 0 & D_1 & 0 & 0 & 0 \\ 0 & C_1^* & 0 & D_1^* & 0 & 0 \\ C_2 & 0 & 0 & 0 & D_2 & 0 \\ 0 & C_2^* & 0 & 0 & 0 & D_2^* \end{bmatrix} \begin{bmatrix} u \\ v \\ u_1 \\ v_1 \\ u_2 \\ v_2 \end{bmatrix} = \lambda \begin{bmatrix} u \\ v \\ u_1 \\ v_1 \\ u_2 \\ v_2 \end{bmatrix}. \quad (41)$$

Calculating the six eigenvalues  $\lambda$  of Eq. (41) and checking if their real part is negative will confirm the stability behavior of the system. As demonstrated in **Fig. 7**, the calculated Lyapunov exponents  $\text{Re}(\lambda)$  are all decaying types, showing that the steady-state solution is stable for all transfer distances of both receivers. The specific function for  $g(|a/\tilde{a}|)$  assumed here does not affect the transfer efficiency if the gain exhibits the above saturation behavior.

### APPENDIX C: POWER TRANSFER MEASUREMENT SETUP

The measurement setup consists of one 68-turn Litz wire transmitter coil with a 30 mm diameter, quality factor of  $Q_{Tx} = 720$ , and intrinsic loss of  $0.55 \Omega$ . Two 35-turn receiver coils were also fabricated with Litz wire with 10 mm diameter and quality factor  $Q_{Rx} = 680$  and intrinsic loss of  $0.078 \Omega$ . The small values for intrinsic loss in coils confirm the initial assumption of negligible loss factors in the receivers in the theoretical calculation and circuit simulation. The value  $G_0 = 0.002 \text{ mS}$ , is the parallel conversion of series loss in the transmitter coil, at  $\omega_0$  and assumed constant for simplicity.

The coupling factor change based on the distance between the transmitter and one receiver coil is shown in **Fig. 8**. The coupling levels between coils were calculated using the COMSOL Multiphysics for magnetic fields simulation of the measuring setup. Transmitter and receivers' inductors coils are in parallel with 330 pF and 3.3 nF capacitors, respectively. In addition, a rack of parallel pins is installed on the transmitter board to add discrete capacitors to tune the resonant frequency of the transmitter. The transmitter part is terminated with a gain realized with an Op-Amp-based circuit shown in **Fig. 9(a)**.

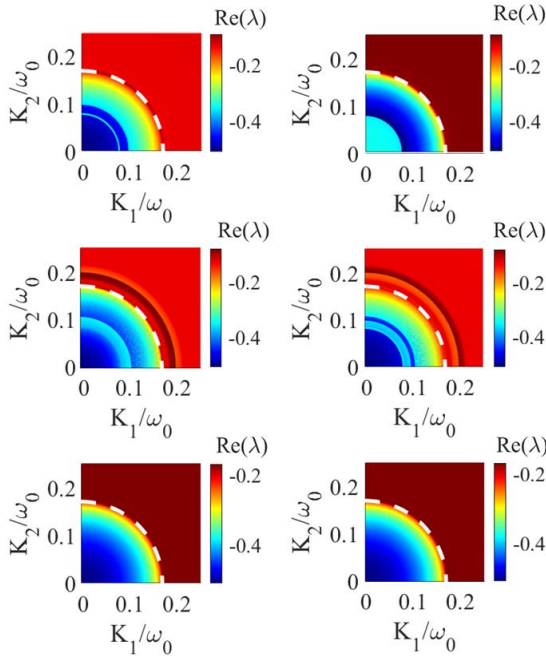


**Fig. 7.** Lyapunov exponents (six solutions of Eq. (41)) to confirm the steady-state solution, versus change of both  $K_1$  and  $K_2$ . For all coupling cases, the real part is always negative which leads to a decaying perturbation always converging to the saturation point. In other, words, the system remains stable for any set of coupling coefficients considered. The circular white dashed line represents the EPD condition  $K_2^2 + K_1^2 = \gamma_r^2$  with the values of  $\gamma_r/\omega_0 = 0.17$  and  $\gamma_0/\omega_0 = 0.001$ .

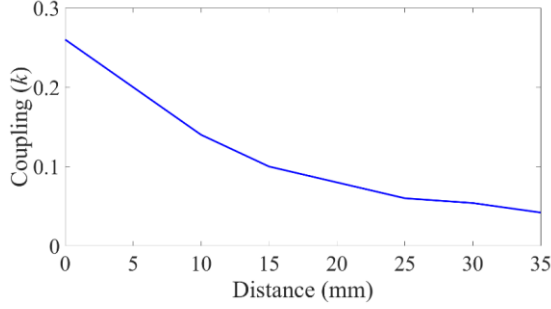
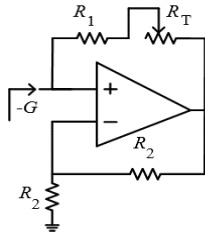
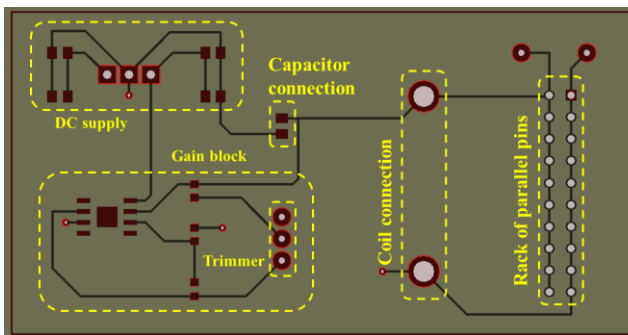


**Fig. 8.** How the mutual inductance coupling factor changes with distance between the transmitter and a receiver.

To realize and tune the negative gain amount, we used an Op-Amp (Analog Devices, model ADA4817), where the negative value is tuned with a trimmer  $R_T$  (Bourns, model 3252W-1-103LF). This block provides negative admittance  $-G_{gain} = -1/(R_1 + R_T)$ , where  $R_1$  is the mount fixed resistance, The  $R_T$  is a trimmer resistance to tune the total feedback resistance ( $R_1 + R_T$ ) in the circuit and bring the negative conductance close to the EPD value based on the required gain for EPD in the theoretical calculation. After trimming the value of  $R_T$  for the required gain, it has been kept



(a)



(b)

**Fig. 9.** (a) Op-Amp configuration to realize the gain  $-G_{gain} = -1/(R_1 + R_T)$ , where the trimmer  $R_T$  is tuned to get the gain value for the system to have an EPD. (b) Printed circuit board layout of the transmitter's circuit where the traces are black, the ground plane underneath is green, and the connecting vias are brown. The blocks in yellow are the DC supply, Gain block, Coil connection, and rack of parallel pins for capacitance adjustments.

fixed in all the experiments. **Figure 9(b)** shows the printed circuit board (PCB) of the assembled circuit, where each block is shown in yellow boxes. All the ground nodes are connected using the bottom green ground layer.

#### APPENDIX D: EPD CONDITION FOR N-RECEIVERS

The concepts provided in this paper can be easily generalized to the " $N$ " number of receivers while maintaining a constant power transfer efficiency for each receiver in their strong coupling region since even with  $N$  number of non-identical receivers, the EPD point still exists. The eigenfrequencies for a  $N + 1$  resonator system with  $g = \gamma_r$  the condition will be

$$\omega_i = \left\{ \begin{array}{l} (N-1)(\omega_0 + i\gamma_r) \\ \omega_0 - \sqrt{K_1^2 + K_2^2 + \dots + K_N^2 - \gamma_r^2} \\ \omega_0 + \sqrt{K_1^2 + K_2^2 + \dots + K_N^2 - \gamma_r^2} \end{array} \right\}. \quad (42)$$

with  $\gamma_{epd} = \sqrt{K_1^2 + K_2^2 + \dots + K_N^2}$ . Although adding more receivers shortens the "high efficiency" region, as shown in **Fig. 10**, still, in the strong coupling range, the system sensitivity to disturbances that change the coupling factor between transmitter and receivers will be reduced.

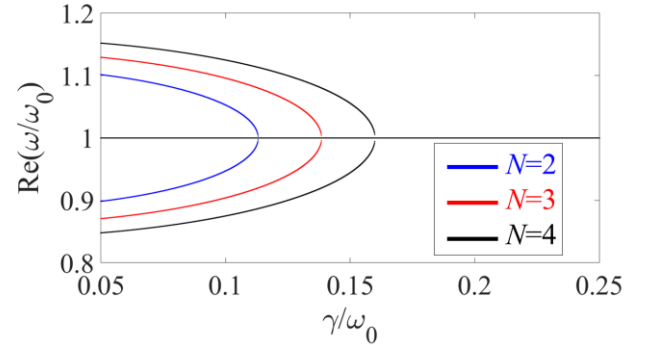


**Fig. 10.** When adding more receivers in system, an EPD can still be found. The value " $N$ " represents the number of receivers.

#### ACKNOWLEDGMENT

This material is based on work supported by the National Science Foundation under award NSF ECCS-1711975.

#### REFERENCES

- [1] A. P. Sample, D. A. Meyer, and J. R. Smith, "Analysis, experimental results, and range adaptation of magnetically coupled resonators for wireless power transfer," *IEEE Transactions on Industrial Electronics*, vol. 58, no. 2, pp. 544–554, Feb. 2011, doi: 10.1109/TIE.2010.2046002.
- [2] A. Kurs, A. Karalis, R. Moffatt, J. D. Joannopoulos, P. Fisher, and M. Soljačić, "Wireless power transfer via strongly coupled magnetic resonances," *Science*, vol.

- 317, no. 5834, pp. 83–86, Jul. 2007, doi: 10.1126/science.1143254.
- [3] A. Hajiaghajani, D. Kim, A. Abdolali, and S. Ahn, "Patterned Magnetic Fields for Remote Steering and Wireless Powering to a Swimming Microrobot," *IEEE/ASME Transactions on Mechatronics*, vol. 25, no. 1, pp. 207–216, Feb. 2020, doi: 10.1109/TMECH.2019.2951101.
- [4] M. Sakhdari, M. Hajizadegan, and P. Y. Chen, "Robust extended-range wireless power transfer using a higher-order PT-symmetric platform," *Physical Review Research*, vol. 2, no. 1, p. 013152, Feb. 2020, doi: 10.1103.
- [5] X. Shu, W. Xiao, and B. Zhang, "Wireless Power Supply for Small Household Appliances Using Energy Model," *IEEE Access*, vol. 6, pp. 69592–69602, 2018, doi: 10.1109/ACCESS.2018.2880746.
- [6] F. Mohseni, P. Marsh, F. Capolino, J. C. Chiao, and H. Cao, "Design of a wireless power and data transfer system for pH sensing inside a small tube," *2021 IEEE Wireless Power Transfer Conference, WPTC 2021*, Jun. 2021, doi: 10.1109/WPTC51349.2021.9458159.
- [7] M. Kiani, U. M. Jow, and M. Ghovanloo, "Design and optimization of a 3-coil inductive link for efficient wireless power transmission," *IEEE Transactions on Biomedical Circuits and Systems*, vol. 5, no. 6, pp. 579–591, Dec. 2011, doi: 10.1109/TBCAS.2011.2158431.
- [8] A. Kurs, A. Karalis, R. Moffatt, J. D. Joannopoulos, P. Fisher, and M. Soljačić, "Wireless power transfer via strongly coupled magnetic resonances," *Science*, vol. 317, no. 5834, pp. 83–86, Jul. 2007, doi: 10.1126/science.1143254.
- [9] J. S. Ho, S. Kim, and A. S. Y. Poon, "Midfield wireless powering for implantable systems," *Proceedings of the IEEE*, vol. 101, no. 6, pp. 1369–1378, 2013, doi: 10.1109/JPROC.2013.2251851.
- [10] W. D. Heiss, "The physics of exceptional points," *Journal of Physics A: Mathematical and Theoretical*, vol. 45, no. 44, p. 444016, Oct. 2012, doi: 10.1088/1751-8113/45/44/444016.
- [11] J. Schindler, A. Li, M. C. Zheng, F. M. Ellis, and T. Kottos, "Experimental study of active LRC circuits with PT symmetries," *Physical Review A*, vol. 84, no. 4, p. 040101, Oct. 2011, doi: 10.1103/PhysRevA.84.040101.
- [12] S. Assaworarith, X. Yu, and S. Fan, "Robust wireless power transfer using a nonlinear parity-time-symmetric circuit," *Nature*, vol. 546, no. 7658, pp. 387–390, Jun. 2017, doi: 10.1038/nature22404.
- [13] M. Sakhdari, M. Farhat, and P. Y. Chen, "PT-symmetric metasurfaces: wave manipulation and sensing using singular points," *New Journal of Physics*, vol. 19, no. 6, p. 065002, Jun. 2017, doi: 10.1088/1367-2630/AA6BB9.
- [14] P. Y. Chen *et al.*, "Generalized parity-time symmetry condition for enhanced sensor telemetry," *Nature Electronics* 2018 1:5, vol. 1, no. 5, pp. 297–304, May 2018, doi: 10.1038/s41928-018-0072-6.
- [15] T. Stehmann, W. D. Heiss, and F. G. Scholtz, "Observation of Exceptional Points in Electronic Circuits," *Journal of Physics A: Mathematical and General*, vol. 37, no. 31, pp. 7813–7819, Dec. 2003, doi: 10.1088/0305-4470/37/31/012.
- [16] H. Hodaie, M. A. Miri, M. Heinrich, D. N. Christodoulides, and M. Khajavikhan, "Parity-time-symmetric microring lasers," *Science*, vol. 346, no. 6212, pp. 975–978, Nov. 2014, doi: 10.1126/SCIENCE.1258480/SUPPL\_FILE/HODAEI.SM.V2.PDF.
- [17] L. Feng, Z. J. Wong, R. M. Ma, Y. Wang, and X. Zhang, "Single-mode laser by parity-time symmetry breaking," *Science*, vol. 346, no. 6212, pp. 972–975, Nov. 2014, doi:10.1126/SCIENCE.1258479.
- [18] D. N. Christodoulides, K. G. Makris, R. El-Ganainy, and Z. H. Musslimani, "Theory of coupled optical PT-symmetric structures," *Optics Letters*, Vol. 32, Issue 17, pp. 2632–2634, vol. 32, no. 17, pp. 2632–2634, Sep. 2007, doi: 10.1364/OL.32.002632.
- [19] M. Feldmaier, J. Main, and F. Schweiner, "Exceptional points of non-Hermitian operators," *Journal of Physics A: Mathematical and General*, vol. 37, no. 6, p. 2455, Jan. 2004, doi: 10.1088/0305-4470/37/6/034.
- [20] A. P. Seyranian, "Sensitivity Analysis of Multiple Eigenvalues," *Mechanics of Structures and Machines*, vol. 21, no. 2, pp. 261–284, Jan. 1993, doi: 10.1080/08905459308905189
- [21] T. Kato, *Perturbation theory for linear operators*, vol. 132. Berlin, Heidelberg: Springer Berlin Heidelberg, 1966. doi: 10.1007/978-3-662-12678-3.
- [22] P. Lancaster, "On eigenvalues of matrices dependent on a parameter," *Numerische Mathematik* 1964 6:1, vol. 6, no. 1, pp. 377–387, Dec. 1964, doi: 10.1007/BF01386087.
- [23] M. I. Vishik and L. A. Lyusternik, "THE SOLUTION OF SOME PERTURBATION PROBLEMS FOR MATRICES AND SELFADJOINT OR NON-SELFADJOINT DIFFERENTIAL EQUATIONS I," *Russian Mathematical Surveys*, vol. 15, no. 3, pp. 1–73, Jun. 1960, doi: 10.1070/RM1960V015N03ABEH004092.
- [24] C. M. Bender and S. Boettcher, "Real Spectra in Non-Hermitian Hamiltonians Having PT Symmetry," *Physical Review Letters*, vol. 80, no. 24, pp. 5243–5246, Jun. 1998, doi: 10.1103/PhysRevLett.80.5243.
- [25] M. v. Berry, "Physics of Non Hermitian Degeneracies," *Czechoslovak Journal of Physics* 2004 54:10, vol. 54, no. 10, pp. 1039–1047, Oct. 2004, doi: 10.1023/B:CJOP.0000044002.05657.04.
- [26] A. Kurs, R. Moffatt, and M. Soljačić, "Simultaneous mid-range power transfer to multiple devices," *Applied Physics Letters*, vol. 96, no. 4, 2010, doi: 10.1063/1.3284651.

- [27] D. Oshmarin, A. F. Abdelshafy, A. Nikzmir, M. M. Green, and F. Capolino, "Experimental demonstration of a new oscillator concept based on degenerate band edge in microstrip circuit, arXiv:2109.07002.[Online].
- [28] X. Zhou and Y. D. Chong, "PT symmetry breaking and nonlinear optical isolation in coupled microcavities," *Optics Express*, vol. 24, no. 7, p. 6916, Apr. 2016, doi: 10.1364/oe.24.006916.